Power Quality Improvement of Synchronous Generators Using an Active Power Filter

Al-Hussein Abu-Jalala*, Tom Cox*, Chris Gerada*, Mohamed Rashed*, Tahar Hamiti† and Neil Brown‡

*Power Electronics, Machines and Control Group
Electrical and Electronic Engineering Department
The University of Nottingham, UK
alhussein.abujalala@nottingham.ac.uk

†Department of Vehicle Electrification
VEDECOM Institute
Versailles 78000, France
tahar.hamiti@vedecom.fr

‡Cummins Power Generation
Peterborough, PE1 5EL
United Kingdom
neil.brown@cummins.com

***Abstract*—Active power filters (APF) are used to improve power quality and are commonly connected in parallel with the load at the point of common coupling (PCC). They are used to compensate for harmonics from nonlinear loads, for reactive power compensation and/or balancing mains currents. This paper will investigate the effect of using an APF to improve the output power quality of a simplified synchronous generator (SSG) with distorted back-EMF. A Matlab Simulink model for the SSG is built to simulate all the system, the APF and the proposed generator. Using an APF, simulation and experimental results show significant improvements in generator output current and reduced the THD in the system.**

***Index Terms*—Synchronous generator, Skewless generator, Active power filter, Four-leg converter.**

I. Introduction

Active power filters (APF) have been used to improve power quality since the 1980s [1]. They are connected in parallel with the load at the point of common coupling (PCC). The main functions of the APF are compensating harmonics from nonlinear loads, balancing source currents and reactive power compensation [2]. Shunt active power filter topologies and control algorithms have been widely discussed in the literature [3]–[6]. In [7]–[10] the APF is used in cases with distorted mains voltages and the results showed a high capability for the proposed control techniques in these papers to eliminate the harmonics in the source current and balance them, regardless of the load condition and source voltage.

The APF is used with stand-alone generators to improve their dynamic performance, where in [11] the APF is used with an isolated synchronous generator feeding a nonlinear load to compensate current harmonics and regulate the generator terminal voltages. In addition, the APF is used to regulate the output voltage of a variable speed interior permanent magnet synchronous generator (IPMSG) with nonlinear load while controlling the reactive power and compensating any current harmonics [12].

The impact of harmonics on a synchronous generator will be apparent both mechanically and electrically. The mechanical effect will appear as vibration on the generator shaft with electromagnetic torque pulsation, and will shorten the lifetime of the generator. The electrical effect will result in distorted current and voltage waveforms in both stator and rotor windings and this will cause excess heating and generator losses, lowering the efficiency of power conversion [13], [14].

The traditional methods to get a good sinusoidal back-emf waveform have been widely reported in literature, such as distributed windings, short-pitching winding, different pole-slot combinations and stator skewing [15], [16], however, these techniques increase generator design complexity and hence cost, and decrease the back-emf voltage. Synchronous generator stators are also commonly skewed to compensate for the slot harmonics, which complicates the manufacturing process.

The purpose of this work is to develop and validate the use of active power filters specifically with simplified synchronous generators. The simplified generators described are less complex and so both faster and less expensive to produce. They permit a higher fundamental emf and so have the potential to produce more power, or to reduce excitation losses and so increase efficiency. However the simplified generator designs also produce significantly more harmonics and so an external method, in this case an APF will be used to mitigate these and ensure the level of harmonics seen at the load remains acceptable.

The additional costs that would be introduced by adding the APF may be compensated by the practical benefits that can be gained. As well as the direct benefits of increased generator capability and reduced construction cost and complexity outlined above, the APF also has established benefits in terms of improving the transient response of the generator [17] and its ride-through capability, as well as the potential to allow reduced power 3 phase output in fault conditions.

In addition, it well known that the cost of semiconductor devices is a decreasing trend, for example, in traction drive systems (55 kW peak power for 18 sec; 30 kw continuous power), the cost of power electronics in 2010 was 7.9 $\$/kW$ and in 2020 This is estimated to drop to 3.3 $\$/kW$, i.e. the cost will be 58% less in ten years [18].

The APF will be used to improve the power quality supplied to the load if the load is linear or compensate load harmonics and balance generator loading when the load is nonlinear.

II. System Configuration

The proposed system is a three-phase four wire system consisting of a simplified synchronous generator (SSG), four leg active power filter (APF), interface L-filter and a load, which may be linear or nonlinear, and balanced or unbalanced as shown in Fig.1.

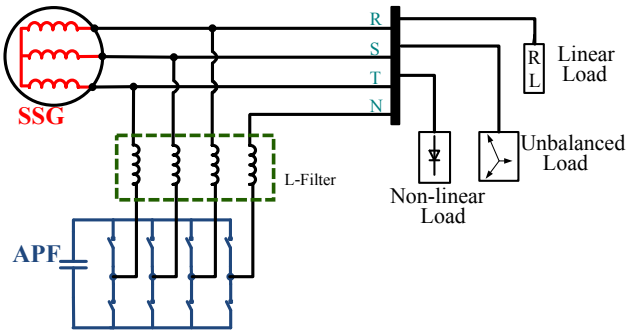

Fig. 1: The proposed system to test the simplified synchronous generator

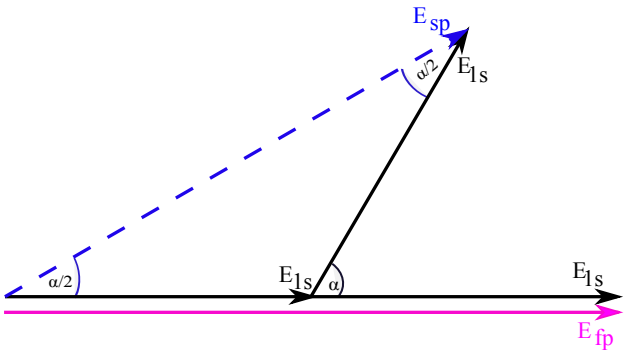

Fig. 3: Phasor diagram of The resultant EMF of the short pitched coil

A. *The Proposed Generator*

The proposed generator is based on a standard commercial 72.5 KVA 4-pole wound field synchronous generator, with modifications made to the stator in order to simplify the manufacturing process and increase the generator capacity. The commercial generator has a $2/3$ pitch winding skewed by one slot pitch, which has 48 slots and a double layer winding, and each phase consists of four coils, with each two connected in parallel and these two then connected in series.

The proposed generator has a skewless stator with a fully pitched winding with the same other parameters of the commercial generator, and is shown in Fig.2. In the proposed generator, the neutral wire is removed to prevent triplen current harmonics from reaching the load. A load side neutral for single phase loads will be supplied from the converter (APF).The parameters of the standard generator and the SSG are given in Table-I.

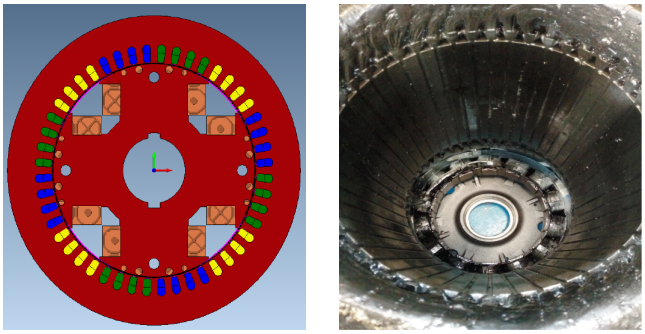

Fig. 2: Full pitch skewless generator (a)2D finite element analysis (FEA) model (b) Experimental prototype (the proposed generator) (c) Stator coil connection diagram

TABLE I: The proposed generator parameters

Element	size
kVA base rating for reactance value	72.5 kVA
Voltage base for reactance value	415/240 V
Stator phase resistance	0.075 Ω
Field winding resistance	0.83 Ω
Direct axis reactance x_d	2.84 pu
Quadratic axis reactance x_q	1.48 pu

According to [19], the fundamental back-EMF of the SG can be written as:

$$E_{rms} = 4.44 f k_d k_p N \Phi_{pole} \tag{1}$$

where f is the induced voltage frequency, k_d is the distribution factor, k_p is the pitch factor, N is the number of turns per phase and Φ_{pole} is the flux per pole. Fig.3 shows the resultant EMF in both short pitched and full pitched coil, where E_{1s} is the induced EMF in one side of the coil. Since the pitch angle in the standard commercial generator is 120^o, and according to equation (2) it has $k_p = 0.866$. Due to the increased pitch factor to 1.0, the back-EMF voltage of the proposed generator will be higher by about 15% than the standard generator at the same flux density.

$$k_p = \frac{\text{Phasor sum of coil side EMFs}}{\text{Arithmatic sum of coil side EMFs}} = \frac{E_{sp}}{E_{fp}}$$
$$k_p = \frac{2E_{1s}\cos(\alpha/2)}{2E_{1s}} = \cos(\alpha/2) \tag{2}$$

The first test done on the proposed generator was the open circuit test. Fig.4 shows the open circuit test curve for both the standard and the proposed modified generator from 2DFEA modelling and experimental tests, along with datasheet values for the standard generator. As can be seen from Fig.4 there is a good match between 2DFEA modelling and measurement results for both generators. In addition, for

the same fundamental output voltage the field current can be reduced from 15 A in the standard generator to 11.2 A in the proposed generator, if the power quality can be maintained.

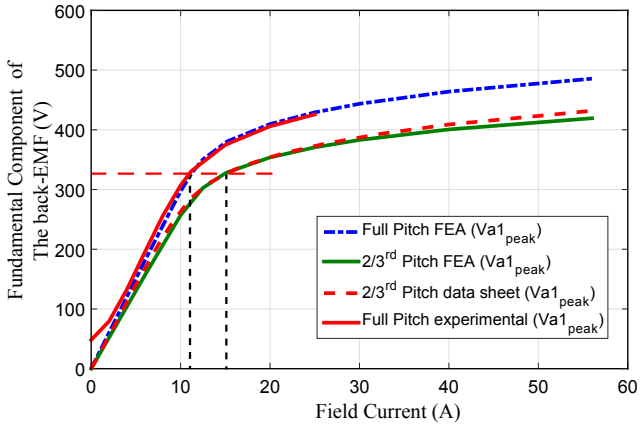

Fig. 4: Open circuit test for the proposed generator and the standard commercial generator

B. Synchronous Generator Model

A Matlab Simulink based model was developed for the proposed generator as shown in Fig.5. This model is based on the inductance matrix of the proposed generator at different rotor positions taken from the 2DFEA model. The inductance matrix is a three dimensional matrix where each layer contains the self and the mutual inductances of the generator coils (i.e. stator, field and damper windings) at one rotor position.

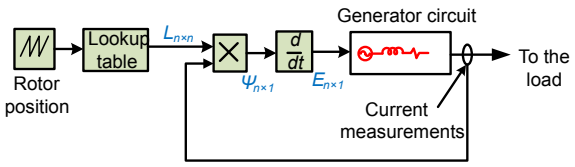

Fig. 5: Block diagram of the generator simulink matlab model

The flux linkage and the induced back-EMF is calculated by (3) and (4) respectively.

$$\Psi_{[n\times1]} = L_{[n\times n]} \times I_{[n\times1]} \tag{3}$$

$$E_{back-EMF[n\times1]} = \frac{d\Psi_{[n\times1]}}{dt} \tag{4}$$

In this model, the effects of saturation were neglected and the field current was assumed to be constant during the simulation time. In order to validate the Simulink model, its performance was first compared to results from both FEA and experiment without the use of an active power filter. Fig.6 shows the comparison between the back-EMF from 2DFEA and the Simulink model. It can be seen that these are in very close agreement between the two models.

In addition, a loaded generator test is done to compare the results from the Matlab Simulink model with the experimental results of the proposed generator, the test is done for a linear

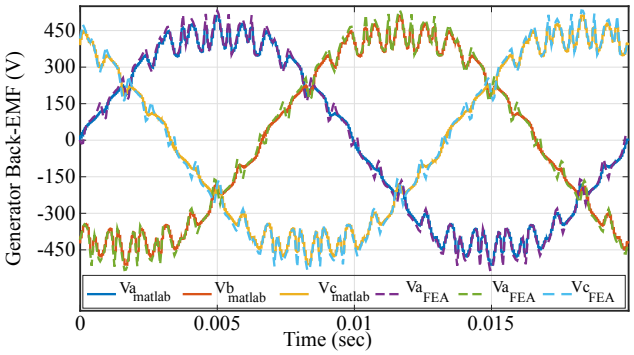

Fig. 6: Comparison between FEA and Matlab models of the proposed generator

$35kW$ resistive load and nonlinear load i.e. three-phase diode bridge with RL load ($R = 9.2\Omega$ and $L = 5.5mH$).
Fig.7. shows the simulation and experimental results for the balanced linear load, the THD in the Simulink model was 4.5%, while in experimental test was 4.1%, a small variation due to the linearity of the simulation.

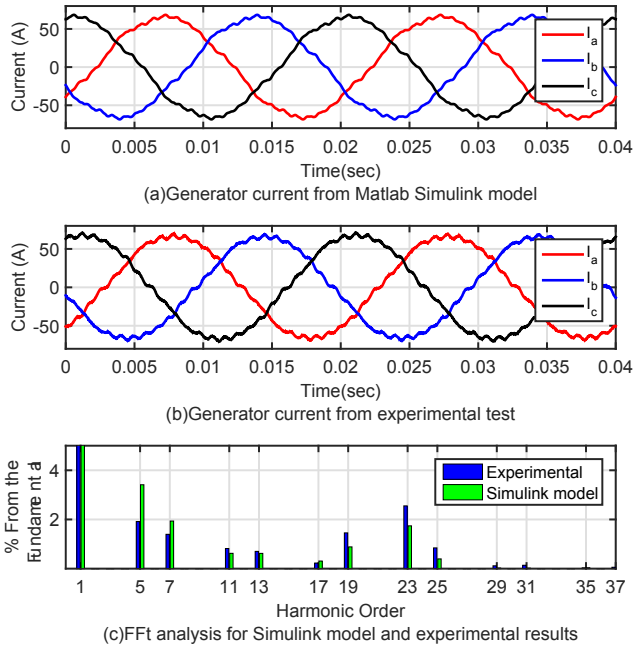

Fig. 7: The simulation and experimental results for balanced linear load (a) Matlab Simulink model (b) experimental result of the proposed generator (C) FFT analysis for simulation and experimental results

Furthermore, the nonlinear load test was done and the results are shown in Fig.8. This figure shows the simulation and experimental results for balanced nonlinear load, as can be seen from the figure, the THD in the Simulink model was 22.3% while in the experimental test this was 25%. As can be seen from Fig.7 and Fig.8 the synchronous generator Simulink model showed a good agreement with the experimental result.

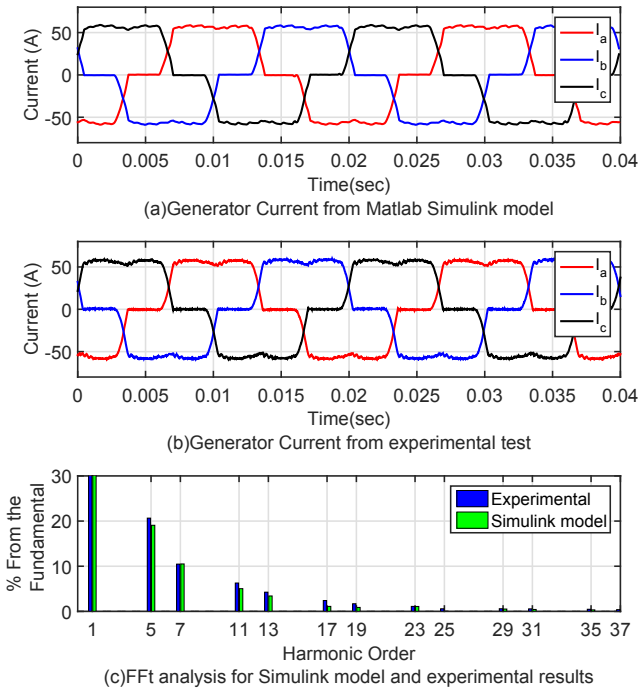

Fig. 8: The simulation and experimental results for balanced non-linear load (a) Matlab Simulink model (b) experimental result of the proposed generator (C) FFT analysis for simulation and experimental results

III. Harmonic Compensation

The APF is the power electronics part in the proposed system, and it is based on a Voltage Source Inverter (VSI). The function of the APF in this system is to compensate the load or the generator current harmonics. This process can be divided to three main steps, which are, phase angle calculation, reference current calculation and APF control. The APF topology and all these steps will be covered in detail in the following subsections.

A. Active Power Filter Topology

In three-phase four-wire system the converter topology can be either a conventional three-phase inverter with DC-link split capacitor with midpoint connection for neutral wire, or a four-leg inverter where the neutral wire is connected to the fourth leg. In this paper the second configuration is chosen to reduce the DC-link size by reducing the rated current and voltage of the DC-link capacitor [20]. In addition, since there is only one capacitor in the four-leg topology, so there is only one voltage to be controlled. However, in the split capacitor with midpoint topology there are two voltages to be regulated and equal to each other, thereby making the control algorithm more complicated [21].

B. Synchronisation Method

An important factor in APF operation is calculating the voltage phase angle at the point of common coupling (PCC), because the other two steps depend on the phase angle calculation. A Phase Locked Loop (PLL) is used to calculate the phase voltage angle. The conventional synchronous reference frame PLL (SFR-PLL) is designed for ideal source voltage and does not give accurate tracking for the phase voltage under non-ideal conditions [22], [23]. In [24] the authors proposed a positive-sequence detector based on a new decoupled double synchronous reference frame phase-locked loop (DDSRF-PLL), this technique is based on positive and negative sequence transformation and detects the phase angle with excellent accuracy when the source has unbalanced voltage. However under distorted voltage source this method still has some error in the detected phase angle. For a good tracking of the phase voltage angle under distorted and unbalanced source a Dual Second order Generalised Integrator PLL (DSOGI-PLL) was proposed in [25]as shown in Fig.9.

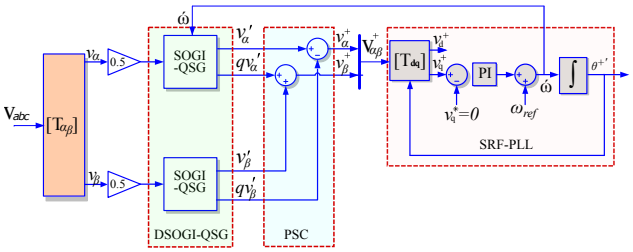

Fig. 9: Block diagram of the DSOGI-PLL

This technique is based on the instantaneous symmetrical components (ISC) in the $\alpha\beta$ coordinates method to detect the positive sequence component.

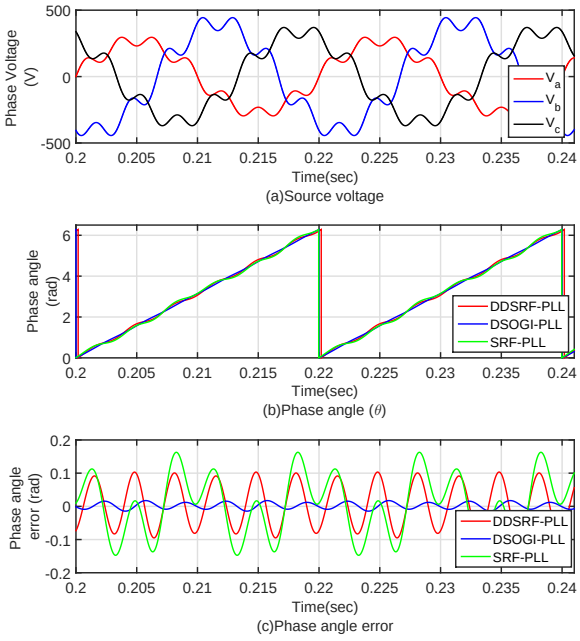

Fig. 10: Simulation results for three different PLLs, (a) source voltages (b) tracked phase angle (c) the error in the tracked angle

Fig.10 shows the simulation result for the different types of PLL. As can be seen on Fig.10(c) there is a significant error in the phase angle tracking in SRF-PLL and DDSFR-PLL while

DSOGI-PLL gives acceptable tracking even in highly distorted voltage source as shown in Fig.10(a)

C. Current Reference Generation Technique

The second stage of APF operation is extracting the reference currents, which are the currents that should be injected at the PCC to compensate current harmonics and get sinusoidal source currents.

The most two widely used methods in APF are Instantaneous power theory (p-q theory) [26], and synchronous reference frame (SRF) d-q technique [27], [28]. SFR-dq is adopted in this paper as it is easier to implement and faster in terms of computation time than the pq theory based technique DSOGI-PLL and gives a very accurate angle. In addition, this technique is considered the best choice amongst four other compensation methods, p-q theory being one of them [28]. The equations from equation (5) to equation (9) summarise SRF-dq technique.

$$\begin{bmatrix} i_d \\ i_q \\ i_0 \end{bmatrix} = M \begin{bmatrix} i_a \\ i_b \\ i_c \end{bmatrix} \tag{5}$$

Where M the transformation matrix (Park transformation)

$$M = \sqrt{\frac{2}{3}} \begin{bmatrix} \cos(\theta) & \cos(\theta - \frac{2\pi}{3}) & \cos(\theta + \frac{2\pi}{3}) \\ -\sin(\theta) & -\sin(\theta - \frac{2\pi}{3}) & -\sin(\theta + \frac{2\pi}{3}) \\ \frac{1}{\sqrt{2}} & \frac{1}{\sqrt{2}} & \frac{1}{\sqrt{2}} \end{bmatrix} \tag{6}$$

Since the controller of the active filter in this system is just dealing with harmonic content, so both i_d and i_q are passed through a high pass filter to get the ac content $\tilde{i_d}$ and $\tilde{i_q}$ in the currents i_d and i_q respectively.

$$i_d \xrightarrow{filter} \tilde{i_d} \Rightarrow i_d^* \tag{7}$$

$$i_q \xrightarrow{filter} \tilde{i_q} \Rightarrow i_q^* \tag{8}$$

$$i_0 \Rightarrow i_0^* \tag{9}$$

where i_d^*, i_q^* and i_0^* are the reference currents are the reference current in d-q axes respectively. To calculate the reference current in abc frame, the inverse Park transformation is used as it is shown in equation (10)

$$\begin{bmatrix} i_a^* \\ i_b^* \\ i_c^* \end{bmatrix} = \sqrt{\frac{2}{3}} \begin{bmatrix} \cos(\theta) & -\sin(\theta) & \frac{1}{\sqrt{2}} \\ \cos(\theta - \frac{2\pi}{3}) & -\sin(\theta - \frac{2\pi}{3}) & \frac{1}{\sqrt{2}} \\ \cos(\theta + \frac{2\pi}{3}) & -\sin(\theta + \frac{2\pi}{3}) & \frac{1}{\sqrt{2}} \end{bmatrix} \begin{bmatrix} i_d^* \\ i_q^* \\ i_0^* \end{bmatrix} \tag{10}$$

The neutral reference current is calculated from equation (11), and the reference voltage for the neutral leg is calculated from equation (12).

$$i_n^* = -(i_a^* + i_b^* + i_c^*) \tag{11}$$

$$v_n^* = -(v_a^* + v_b^* + v_c^*) \tag{12}$$

D. Current Control Technique

The function of the current controller is generating the voltage reference for the VSI to produce a current equal to the calculated reference current. Then this current is absorbed or injected from/into the PCC to eliminate the harmonics from the generator/load current.

The PI controller (SRF-PI) in the d-q reference frame gives good results in DC values where it drives the steady state to zero. However, in this system the reference current is an AC waveform so SRF-PI controller is not the optimum choice for the controller.

For AC waveforms the proportional resonant current controller (PR) has been widely used due to its capability for regulating AC waveforms [29]. This controller is implemented in stationary reference frame ($\alpha - \beta$) plane and it has a high performance in tracking sinusoidal reference currents. The transfer function on non-ideal PR is given in equation (13)

$$G_{AC}(s) = k_p + \frac{2k_i\omega_c s}{s^2 + 2\omega_c s + \omega^2} \tag{13}$$

Where k_p is the proportional controller gain, k_i is the integral controller gain and ω_c is the cut-off frequency.

To include the harmonics in the controller, selective harmonic compensators can be cascaded with the PR controller, each harmonic has a resonant block and this block is tuned at the harmonic frequency. The transfer function of the harmonic compensator is given as:

$$G_h(s) = \sum_{h=5,7,11,\ldots} \frac{2k_{ih}\omega_c s}{s^2 + 2\omega_c s + (h\omega)^2} \tag{14}$$

The harmonics that need to be compensated in this system are $h = 5, 7, 11, 13, 17, 19, 23$ and 25, these being most dominant harmonics in the proposed generator. Fig.11 shows the block diagram of PR-HC current controller

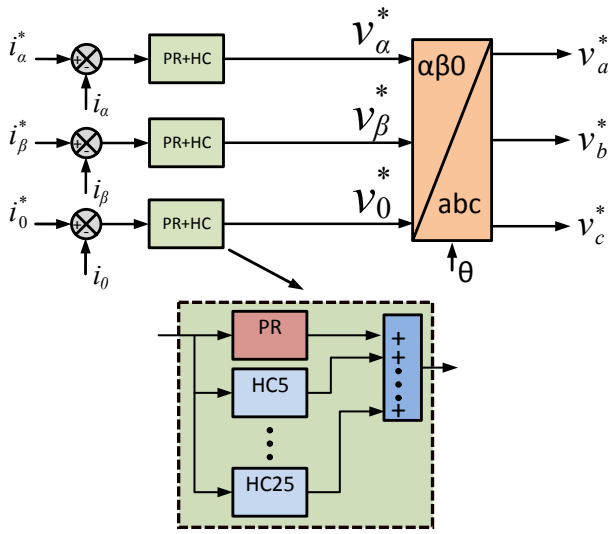

Fig. 11: Block diagram of PR+HC current controller

IV. Simulation Results

This simulation was carried out for the system in Fig.1 with interface filter ($4.2\ mH$) and three different load types: Linear, balanced nonlinear and unbalanced nonlinear load. All three tests used a constant excitation and generator speed. The switching frequency was $10kHz$ in all simulations and the simulation time was $5\ sec$, with the APF enabled at $t = 2\ sec$ to give a clear indication of system behaviour both with and without the APF. The PR+HC controller parameters that were used in the simulation are given in Table-II. The current waveforms of the generator, load, and the APF were analysed.

TABLE II: The PR+HC controller parameters

Element	Size
K_p	7
k_I	250
k_{Ih}	250

A. Balanced Linear Load

In this simulation a linear load was connected to the generator ($35\ kW$) at rated voltage $415\ V$ line to line. The output generator current, load current and filter current are show in Fig.12.With the APF in operation, the total harmonic distortion (THD) of the load currents is reduced from 4.5% to around 2.1%.

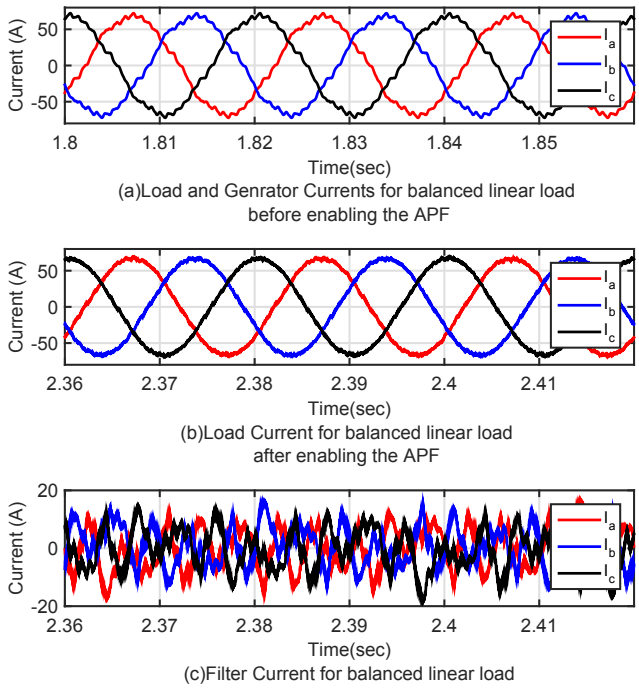

Fig. 12: Generator, load, and filter currents with linear balanced load

B. Balanced Non-Linear Load

To simulate a nonlinear balanced load a three phase diode bridge with RL load ($L = 5.5\ mH$ and $R = 9.4\ \Omega$) was connected to the generator. When the APF was enabled, the THD in the generator current decreased from 22.3% before switching APF on to 3.43% after switching APF on. Fig.13 shows the generator, the load and the filter current before and after the compensation.

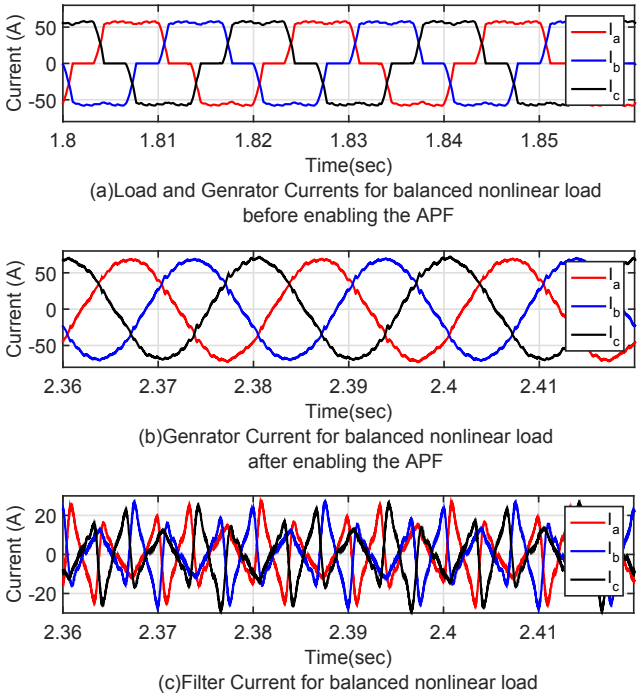

Fig. 13: Generator, load, and filter currents with nonlinear balanced load

C. Unbalanced Non-Linear Load

The simulation was undertaken for two different types of unbalanced load. In the first type the sum of the three phase currents is zero (Just negative sequence components). In the second type, the sum of the three phase current is not zero i.e. there is a current in the neutral wire (negative and zero sequence components).

1) Unbalanced Non-Linear Load with Only Negative Sequence Components (Type-1): To simulate the first type of unbalance, (only negative sequence), a nonlinear load (full bridge diode rectifier) is added to the circuit of subsection IV-B and connected between phase-A and phase-B. The DC load was $L = 5.5\ mH$ and $R = 27\ \Omega$. The simulation results are shown in Fig.14, as can be seen from the figure, when the APF is enabled the generator current became balanced and the THD significantly improved. For example, the THD in phase-C drops from 20.1% to 3.8%. Table-III summarises the THD and the current values of the system before and after enabling the APF.

2) Unbalanced Non-Linear Load with negative and zero sequence components (type-2): In this simulation a single-phase load is added to the simulation in subsection IV-B and connected between phase A and the fourth leg of the converter (neutral point). As can be seen from Fig.15 the APF decreased THD in the generator current to 22.3% to 3.65% and supplied the single phase load when it was connected.

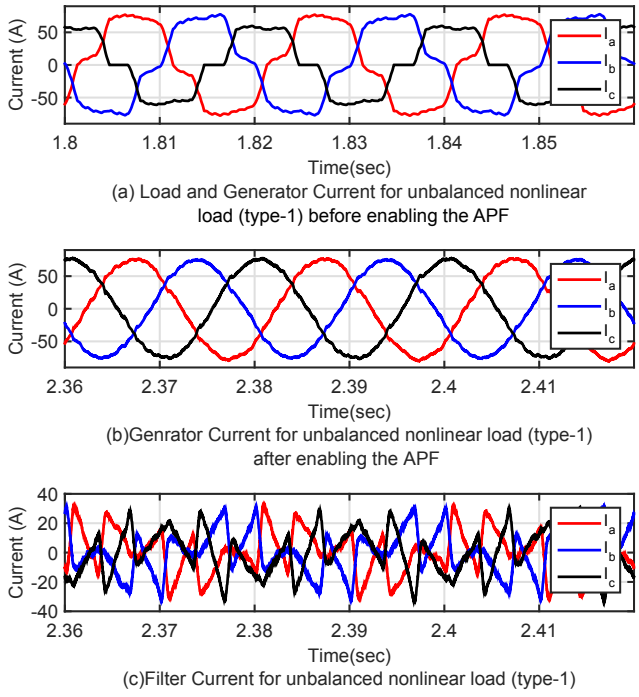

Fig. 14: System currents after enabling the APF with nonlinear and unbalanced load type-1

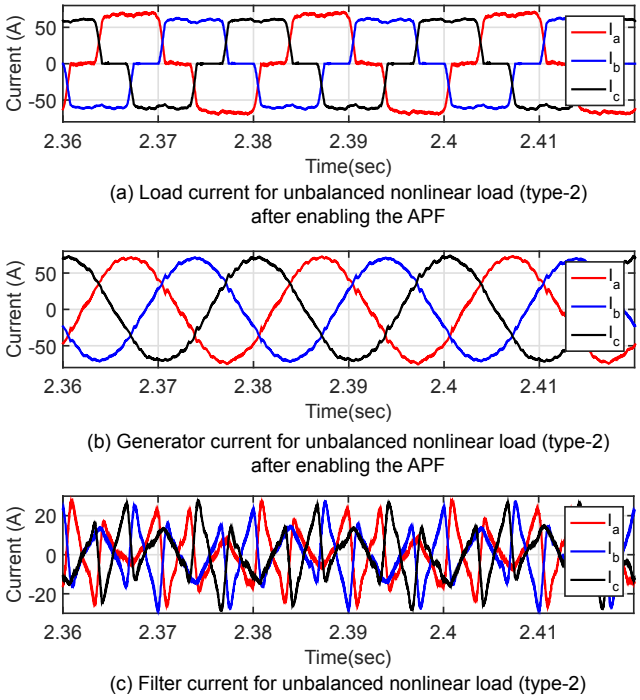

Fig. 15: System currents after enabling the APF with nonlinear and unbalanced load type-2

TABLE III: The simulation results for the THD and currents values before and after enabling the APF for unbalanced nonlinear load with just negative sequence

	Before enabling the APF		After enabling the APF			
	load/generator		Load		Generator	
	THD%	Amp	THD%	Amp	THD%	Amp
Phase-A	14.6	57.5	20.3	60.0	3.7	54.6
Phase-B	15.4	56.5	19.7	58.9	3.3	52.9
Phase-C	20.1	45.4	25.5	47.1	3.8	53.7

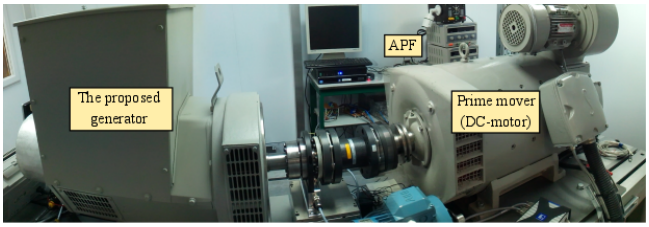

Fig. 16: The experimental test rig

V. EXPERIMENTAL RESULTS

The test bed consists of a simplified synchronous generator with a skewless stator and a full pitch winding as shown in Fig.2(b) coupled with a DC-motor driven by a Eurotherm Drive, a 590 Digital series with closed loop speed Control, (used to maintain a constant rotational speed) and an active power filter as shown in Fig.16. For the excitation, the field winding was fed directly by using an external DC source through slip rings on the rotor shaft.

The active power filter is shown in Fig.17, which is a four-leg IGBT converter constructed in the lab by using two commercial three-phase SKAI modules, designed by Semikron for automotive applications, (SKAI45A2GD12-W24DI) [30]. These two converters are connected in parallel with one DC-link capacitor, where only one leg was used from the second SKAI module. The APF circuit parameters are given in Table-IV. The control platform that is used experimentally to implement the active power filter controller is composed of FPGA (Field Programmable Gate Array), DSP (Digital Signal Processor) and DSK6713HPI daughtercard (TMS320C6713). The control algorithm is implemented in the DSP by using Code Composer Studio, and this program calculates the reference signals for the APF. Then the FPGA takes these reference signals and generate the gate pulses for the APF switches.

TABLE IV: The APF parameters

Element	Size
Switching frequency	10 kHz
L-filter inductance	4.2 mH
DC-link capacitor	5 mF
DC-link voltage	730 V

A. Balanced Linear Load

In this test, a three-phase resistive load (35 kW) was connected to the generator and the load currents without and with APF are shown in Fig.18(a) and Fig.18(b) respectively. As can be seen from the figure when the APF enabled the THD in load current has decreased from (4.1%) to (1.9%).

B. Balanced Non-Linear Load

To represent the balanced and nonlinear load a three-phase diode rectifier connected to RL load ($L = 5.5\ mH$ and

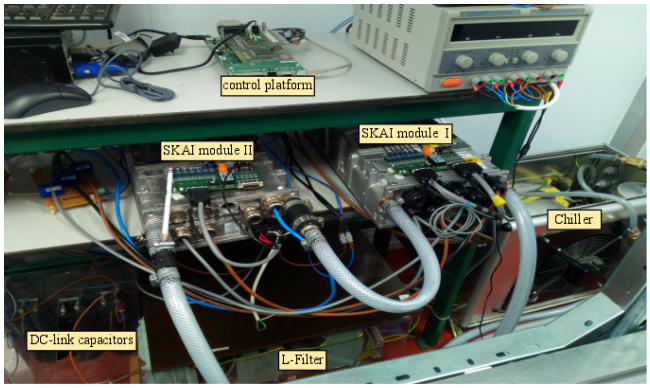

Fig. 17: The active power filter and its accessories: L-filter, DC-link capacitor and chiller

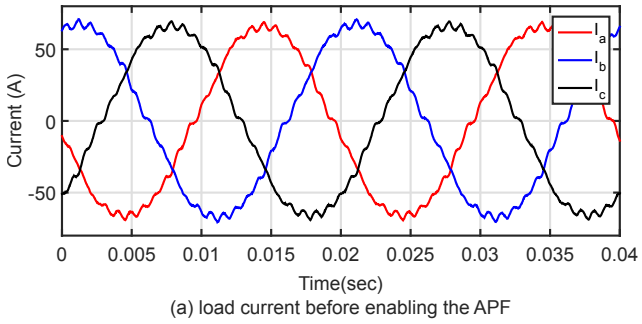

Fig. 18: Load current with 35 kW resistive load in experimental test

$R = 9.4\ \Omega$) was used as a load. The aim of this test to see to what extent the APF can improve the generator output current. Fig.19 shows the generator current before and after enabling the APF. As can be seen from the figure the APF had dramatically improved the generator current and the THD became (5%) instead of (24.7%)before it enabled.

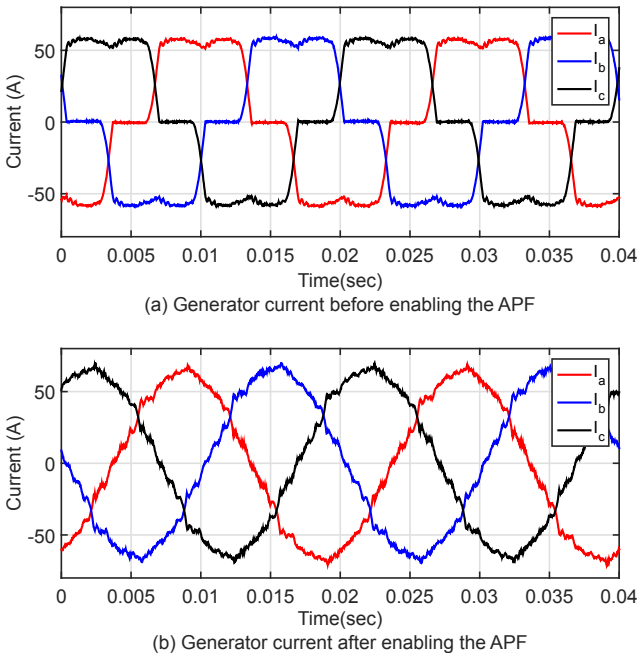

Fig. 19: Experimental result: generator currents before and after enabling the APF

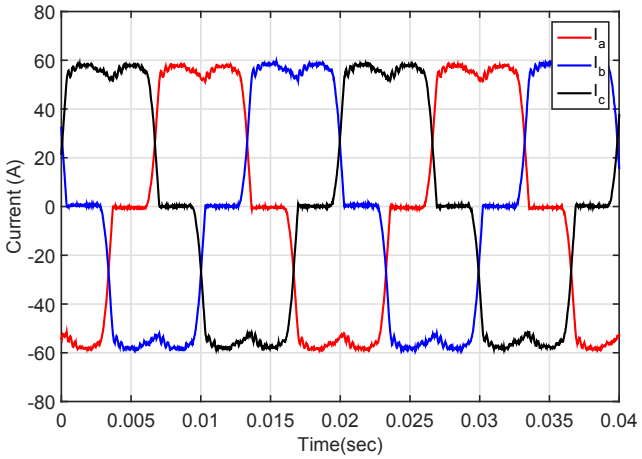

Fig. 20: Generator/ load current before enabling the APF

TABLE V: Generator/load currents before the APF enabled

Phase-A	Phase-B	Phase-C
47.4A	48.4A	46.7A

C. Unbalanced Non-Linear Load-type(2)

The load was constructed from: A three-phase diode rectifier connected to RL load ($L = 5.5\ mH$ and $R = 9\ \Omega$). A single-phase load (30Ω) connected between phase A and APF neutral leg. The total power was about $34.5Kw$. When the generator started the load was connected and the APF disabled. So the single phase-load is OFF because the neutral is disconnected (the neutral wire is supplied through the APF). The current waveforms for both the generator and the load are as shown in Fig.20. The phase currents are as given in Table-V and the THD was (25%). When the APF is enabled, the single-phase load is supplied and this gives unbalanced loading in the load side, but in the generator side, the APF compensated the harmonics in the generator currents and balanced them. Fig.21 shows the load and the generator currents after enabling the APF respectively. As can be seen from Fig.22 the THD in generator current has improved and decreased from (25%) before switching on the APF to about (5.8%) after switching on the APF. Also, the APF decreased the unbalanced loading in the generator current. Table-VI shows the difference in THD and unbalanced loading in the generator and load current before and after enabling the APF.

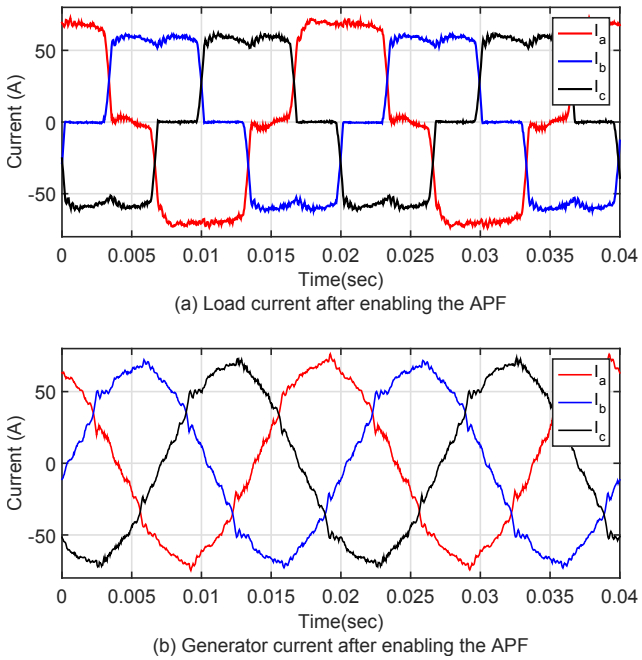

(a) Load current after enabling the APF

(b) Generator current after enabling the APF

Fig. 21: System currents after enabling the APF with nonlinear and unbalanced load

TABLE VI: The experimental results for the THD and currents values before and after enabling the APF for unbalanced nonlinear load

	Before enabling the APF		After enabling the APF			
	load/generator		Load		Generator	
	THD%	Amp	THD%	Amp	THD%	Amp
Phase-A	25.1	47.4	22.8	57.4	5.7	51.6
Phase-B	24.8	48.4	27	49.3	5.3	52.8
Phase-C	25	46.7	26.8	47.5	5.9	50.2

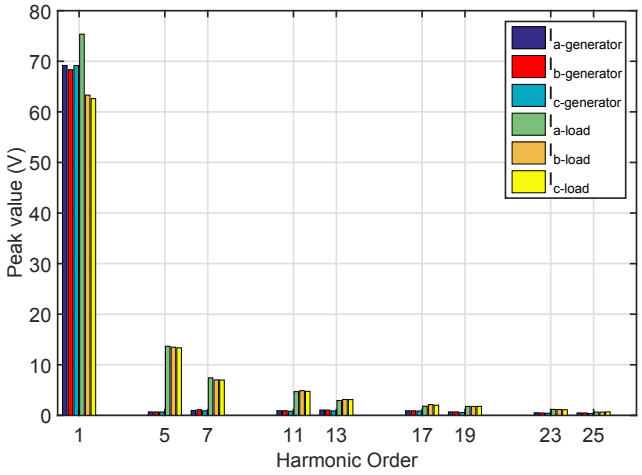

Fig. 22: FFT for generator and load currents after the APF enabled with nonlinear and unbalanced load

VI. Discussion

In the previous two sections the simulation and experimental results were presented, and the experimental results have supported the simulation results in the three cases. For the first case, balanced linear load, the THD in the load current after enabling the controller in the simulation was (2.1%) and it is close to the experimental result which was (1.9%) see Fig.12 and Fig.18 respectively. In the second case, balanced nonlinear load, also the simulation results and experimental results had good agreement, where in the simulation the THD in the generator current was (3.4%), while in the experimental result was (5%), as can be seen from Fig.13 and Fig.19 . Finally in the third case, unbalanced nonlinear load (type-2), also the THD in the simulation result was (3.65%) and in the experimental result was (5.8%) as shown in Fig.15 and Fig.21 respectively, and the APF supplied the single-phase load while maintaining the generator current balance as shown in Table-VI. Table-VII summarises the comparison between the simulation results and experimental results in the three different cases.

TABLE VII: Comparison between the simulation results and the experimental results for the THD in the load/generator current

	Before APF enabled		After APF enabled	
	Sim.	Exp.	Sim.	Exp.
Balanced Linear load (Load)	4.5 %	4.1%	2.1 %	1.9%
Balanced Nonlinear Load (Generator)	22.3%	25%	3.4%	5.0%
Unbalanced Nonlinear Load (Generator)	22.3%	25%	3.6%	5.8%

VII. Conclusions

The effect of using an active power filter to compensate for the poor harmonic output of a simplified synchronous generator has been investigated by both simulation and experiment. The experimental results have validated the simulation results and shown that the APF can be integrated with a simplified synchronous generator to provide an acceptable level of power quality to the load from a simple generator with a poor quality output waveform at the point of common coupling (PCC). While this system achieved a satisfactory level of power quality in terms of THD, for the systems that require more restricted THD values such as micro grids, the proposed system THD could be improved by using an LCL-interface filter instead of L-filter, increasing the switching frequency above $10kHz$ or the use of other types of controllers

The novelty of this work is the use of the APF to allow the simplification of the design of the synchronous generator, allowing the generator capacity and/or efficiency to be increased, and further permitting a simplified design that is both less expensive and faster to produce while maintaining an acceptable level of power quality at the load.

As well as the benefits defined above, the use of APF to compensate for poor generator output power quality is particularly apt for the use of fractional slot concentrated windings, allowing for decreased end winding length and fully automated coil winding and placement, while compensating for the windings natural high harmonic content. The APF may also be used to improve transient response during sudden changes in generator loading and improve fault ride-through capability.

Acknowledgement

The authors gratefully acknowledge the support of the Ministry of Higher Education and Scientific Research - Libya,

the University of Nottingham, and Cummins Generator Technologies in carrying out this research.

REFERENCES

[1] D. Chen and S. Xie, "Review of the control strategies applied to active power filters," in *IEEE International Conference on Electric Utility Deregulation, Restructuring and Power Technologies. Proceedings*, vol. 2, April 2004, pp. 666–670 Vol.2.

[2] H. Akagi, "New trends in active filters for power conditioning," *IEEE Transactions on Industry Applications*, vol. 32, no. 6, pp. 1312–1322, Nov 1996.

[3] M. El-Habrouk, M. K. Darwish, and P. Mehta, "Active power filters: a review," *IEE Proceedings - Electric Power Applications*, vol. 147, no. 5, pp. 403–413, Sep 2000.

[4] H. L. Jou, K. D. Wu, J. C. Wu, C. H. Li, and M. S. Huang, "Novel power converter topology for threephase four-wire hybrid power filter," *IET Power Electronics*, vol. 1, no. 1, pp. 164–173, March 2008.

[5] M. I. M. Montero, E. R. Cadaval, and F. B. Gonzalez, "Comparison of control strategies for shunt active power filters in three-phase four-wire systems," *IEEE Transactions on Power Electronics*, vol. 22, no. 1, pp. 229–236, Jan 2007.

[6] P. Dey and S. Mekhilef, "Current controllers of active power filter for power quality improvement: A technical analysis," *Automatika–Journal for Control, Measurement, Electronics, Computing and Communications*, vol. 56, no. 1, 2015.

[7] S.-J. Huang and J.-C. Wu, "A control algorithm for three-phase three-wired active power filters under nonideal mains voltages," *IEEE Transactions on Power Electronics*, vol. 14, no. 4, pp. 753–760, Jul 1999.

[8] P. Salmeron and R. S. Herrera, "Distorted and unbalanced systems compensation within instantaneous reactive power framework," *IEEE Transactions on Power Delivery*, vol. 21, no. 3, pp. 1655–1662, July 2006.

[9] C.-C. Chen and Y.-Y. Hsu, "A novel approach to the design of a shunt active filter for an unbalanced three-phase four-wire system under nonsinusoidal conditions," *IEEE Transactions on Power Delivery*, vol. 15, no. 4, pp. 1258–1264, Oct 2000.

[10] X. Yuan, W. Merk, H. Stemmler, and J. Allmeling, "Stationary-frame generalized integrators for current control of active power filters with zero steady-state error for current harmonics of concern under unbalanced and distorted operating conditions," *IEEE Transactions on Industry Applications*, vol. 38, no. 2, pp. 523–532, Mar 2002.

[11] T. Sürgevil and E. Akpinar, "Application of shunt active power filter to isolated synchronous generator system," in *35th Annual Conference of IEEE Industrial Electronics*, Nov 2009, pp. 249–254.

[12] K. Nishida, T. Ahmed, and M. Nakaoka, "Advanced active power filter controlled permanent-magnet synchronous generator for automotive applications," in *IEEE Power Electronics Specialists Conference*, June 2007, pp. 1508–1514.

[13] J. q. Wang, P. c. Song, C. h. Cui, J. k. Li, and T. Yang, "Analysis of operation of synchronous generator under the distortion of harmonic current," in *Asia-Pacific Power and Energy Engineering Conference*, March 2012, pp. 1–4.

[14] W. Fan and Y. Liao, "Impacts of flickers, harmonics and faults on synchronous generator operations," in *Proceedings of the 2012 44th Southeastern Symposium on System Theory (SSST)*, March 2012, pp. 220–225.

[15] D. A. Kocabas, "Novel winding and core design for maximum reduction of harmonic magnetomotive force in ac motors," *IEEE Transactions on Magnetics*, vol. 45, no. 2, pp. 735–746, Feb 2009.

[16] H. Asgharpour-Alamdari, Y. Alinejad-Beromi, and H. Yaghobi, "Reduction in distortion of the synchronous generator voltage waveform using a new winding pattern," *IET Electric Power Applications*, vol. 11, no. 2, pp. 233–241, 2017.

[17] A. Abu-Jalala, T. Cox, C. Gerada, M. Rashed, T. Hamiti, and N. Brown, "Performance improvement of simplified synchronous generators using an active power filter," in *IEEE Energy Conversion Congress and Exposition (ECCE)*, Oct 2017, pp. 1845–1849.

[18] "Vehicle technologies multi-year program plan 2011-2015; section 2:2:1," https://www1.eere.energy.gov/vehiclesandfuels/pdfs/program/vt_mypp_2011-2015.pdf, accessed: 2018-03-01.

[19] C.-M. Ong, *Dynamic Simulation of Electric Machinery Using Matlab/Simulink*. Prentice Hall PTR Upper Saddle River, NJ, 1998.

[20] C. A. Quinn and N. Mohan, "Active filtering of harmonic currents in three-phase, four-wire systems with three-phase and single-phase nonlinear loads," in *Applied Power Electronics Conference and Exposition, 1992. APEC '92. Conference Proceedings 1992., Seventh Annual*, Feb 1992, pp. 829–836.

[21] C. A. Quinn, N. Mohan, and H. Mehta, "A four-wire, current-controlled converter provides harmonic neutralization in three-phase, four-wire systems," in *Proceedings Eighth Annual Applied Power Electronics Conference and Exposition,*, Mar 1993, pp. 841–846.

[22] V. Kaura and V. Blasko, "Operation of a phase locked loop system under distorted utility conditions," *IEEE Transactions on Industry Applications*, vol. 33, no. 1, pp. 58–63, Jan 1997.

[23] S.-K. Chung, "A phase tracking system for three phase utility interface inverters," *IEEE Transactions on Power Electronics*, vol. 15, no. 3, pp. 431–438, May 2000.

[24] P. Rodriguez, J. Pou, J. Bergas, J. I. Candela, R. P. Burgos, and D. Boroyevich, "Decoupled double synchronous reference frame pll for power converters control," *IEEE Transactions on Power Electronics*, vol. 22, no. 2, pp. 584–592, March 2007.

[25] P. Rodriguez, R. Teodorescu, I. Candela, A. V. Timbus, M. Liserre, and F. Blaabjerg, "New positive-sequence voltage detector for grid synchronization of power converters under faulty grid conditions," in *Power Electronics Specialists Conference*, 2006, pp. 1–7.

[26] H. Akagi, Y. Kanazawa, and A. Nabae, "Instantaneous reactive power compensators comprising switching devices without energy storage components," *IEEE Transactions on Industry Applications*, vol. IA-20, no. 3, pp. 625–630, May 1984.

[27] P. Santiprapan and K. L. Areerak, "Performance improvement of harmonic detection using synchronous reference frame method," in *2010 International Conference on Advances in Energy Engineering*, June 2010, pp. 52–55.

[28] G. D. Marques, "A comparison of active power filter control methods in unbalanced and non-sinusoidal conditions," in *Industrial Electronics Society, 1998. IECON '98. Proceedings of the 24th Annual Conference of the IEEE*, vol. 1, Aug 1998, pp. 444–449 vol.1.

[29] R. Teodorescu, F. Blaabjerg, M. Liserre, and P. C. Loh, "Proportional-resonant controllers and filters for grid-connected voltage-source converters," *IEE Proceedings - Electric Power Applications*, vol. 153, no. 5, pp. 750–762, September 2006.

[30] Semikron, *Three-pase IGPT INverter SKAI 45A2GD12-W24DI*, 2011.

Al-Hussein Abu-Jalala received the bachelor's degree in electrical and electronic engineering in 1996 from Omar Al-Mukhtar University, Al Bayda, Libya, and the M.Sc. degree in electrical engineering 2012 from Misurata University, Misurata, Libya. He is currently working toward the Ph.D. degree at the Power Electronics, Machines and Control Group, Department of Electrical and Electronic Engineering, The University of Nottingham, Nottingham, U.K.

His current research interests included analysis and design of salient-pole Synchronous generators and active power filters.

Tom Cox (M'09) received the Ph.D. degree in the development of novel linear machines from The University of Bath, Bath, U.K., in 2009. He subsequently worked in industrial research and development on linear drive systems, electromagnetic actuators, and electromagnetic launch systems for aircraft. In 2014, he was appointed as an Assistant Professor of electrical machines at The University of Nottingham, Nottingham U.K. His main research interests include the design and development of electromagnetic launch systems and actuators, integrated machine and drive systems, and novel winding configurations.

Chris Gerada (M'05-SM'14) received the Ph.D. degree in numerical modeling of electrical machines from The University of Nottingham, Nottingham, U.K., in 2005. He subsequently worked as a Researcher with the University of Nottingham on high performance electrical drives and on the design and modeling of electromagnetic actuators for aerospace applications. Since 2006, he has been the Project Manager of the GE Aviation Strategic Partnership. In 2008, he was appointed as a Lecturer in electrical machines; in 2011, as an Associate Professor; and in 2013, as a Professor at The University of Nottingham. His main research interests include the design and modeling of high-performance electric drives and machines.

Prof. Gerada serves as an Associate Editor of the IEEE TRANSACTIONS ON INDUSTRY APPLICATIONS and is the Chair of the IEEE Industrial Electronics Society Electrical Machines Committee.

Mohamed Rashed (M'07) received the Ph.D. degree in electrical motor drives from the University of Aberdeen, Aberdeen, U.K., in 2002. He was a Post-Doctoral Research Fellow with the Department of Engineering, University of Aberdeen for the periods, from 2002 to 2005 and from 2007 to 2009. In 2005, he was appointed as an Assistant Professor with the Department of Electrical Engineering, Mansoura University, Mansoura, Egypt, and then on leave from 2007. In 2008, he was promoted to an Associate Professor in Mansoura University, Egypt. In 2009, he joined the Power Electronics, Machines and Control Research Group, Department of Electrical and Electronic Engineering, The University of Nottingham, Nottingham, U.K., where he is currently a Senior Research Fellow. His current research interests include the design and control of electrical motor drives and power systems for aerospace applications, power electronics for micro grids, renewable energy sources, and energy storage systems.

Tahar Hamiti was born in Larbàa Nath Irathen, Algeria, in 1979. He received the Ingénieur d'Etat degree in automatic control systems from the University of Tizi-Ouzou, Tizi-Ouzou, Algeria, and the Ph.D. degree in electrical engineering from the University of Nancy I, Nancy, France. From 2010 to 2015, he was a Research Fellow and subsequently a Lecturer within the Power Electronics, Machines and Control Group, The University of Nottingham, UK. In 2015 Dr Hamiti joined VEDECOM, a French institute for energy transition to work on novel electrical machines for electric and hybrid vehicles. His research interests include modeling, optimal design, and control of high-performance electrical machines for transportation applications and power generation.

Neil Brown received the graduate degree in electric/electronic engineering from Nottingham Trent University, Nottingham, U.K., in 1991, and the Ph.D. degree in electrical machines from Durham University, Durham, U.K., in 2003. He is currently a Visiting Professor with The University of Nottingham, Nottingham. He joined Cummins in 1995, and is the Chief Engineer Stamford Products, Cummins Generator Technologies, Stamford, U.K. While at Cummins, he has held various roles, including Applications Engineer, Electromagnetic Design Engineer, Research Manager, Chief Engineer for Stamford Products, Chief Engineer Research and Technology, and the Director, Advanced Electrical Machines, before returning to his role as a Chief Engineer Stamford Products in 2016. Before his time at Cummins, he ran his own electrical business, was a College Lecturer, and worked for GEC on projects up to 100 MVA. He is the author of 80 publications, named inventor of 11 patents, and the co-inventor of the Haydock Brown Machine.

Dr. Brown is a certified Six Sigma Green Belt and Sponsor, a Chartered Engineer, in the U.K. and a Fellow of the Institution of Engineering and Technology, U.K.